Optimized Thermodynamics and Building Physics of large-scale Thermal Energy Storage

Alice Tosatto[1], Fabian Ochs[1], Christoph Muser[2] and Franz Hengel[3]

[1] Unit of Energy Efficient Building, Universität Innsbruck, Innsbruck (Austria)

[2] Ingenieurbüro ste.p ZT-GmbH, Vienna (Austria)

[3] AEE Intec, Gleisdorf (Austria)

Abstract

Seasonal thermal energy storage (TES) systems are a key element to promote the increase of renewable energy in district heating networks. Their complex dynamic operation within the energy system as well as their interaction with the surrounding environment requires detailed planning and design. The TES envelope plays a key role: the TES efficiency and the temperature of the surrounding ground are strongly influenced by the thermal losses through the cover and walls. Numerical simulations are a fundamental step to define the baseline targets for the optimal TES performance. Materials testing are required to assess the effective performance of the selected materials under the specific TES operating conditions and to support the design of the specific envelope performance. The construction of mock-ups is a third element to verify the test results and to identify possible challenges in the real scale application. In this work, these three elements are mutually integrated to support the design and optimization of the final TES structure with particular attention in preventing the formation of convective heat flux within the insulation layer.

Keywords: Thermal energy storage, thermal losses, thermal insulation, porous insulation, numerical modelling, convective heat transfer

1. Introduction

The decarbonization of the building sector requires the integration in the energy system of renewable energy (RE) sources, traditionally characterized by high volatility, low density and often strong daily and seasonal oscillations. Alongside the transition of the energy generation systems, storage systems will gain increasing importance to ensure the stability of the energy supply and to increase the self-sufficiency of the communities, as it allows to decouple energy demand and generation (Golmohamadi et al., 2022).

In district heating (DH) networks, large-scale water-based thermal energy storage (TES) systems have been used to increase the share of RE. The two main construction solutions can be distinguished between tank TES (TTES) and pit TES (PTES) (Schmidt et al., 2018). TTES are of cylindrical shape and are usually freestanding; some examples are the TTES of Munich Ackermannbogen (see Fig. 1(a)) and Friedrichshafen (Ochs, 2009). PTES have a truncated pyramidal shape, generally present significantly larger volumes than TTES and can be considered the current state of the art of water-based TES, with the main examples being the PTES in Dronninglund, Marstal and the more recent Høje Taastrup in Denmark and new plant in Langkazi (Tibet, China) (International Energy Agency (IEA), 2024).

The successful application in Denmark has increased the interest in the use of this technology in other countries, but the local specific requirements (i.e., presence of groundwater, low space availability) need the implementation of specific solutions (i.e., lateral insulation, diaphragm walls, graphically presented in Fig. 1(b)) that can be cost demanding (Tosatto, Ochs, Dahash, & Muser, 2022). The TES planning and design requires the evaluation of these requirements at different levels, from the DH grid to the specific envelope element. In this phase, numerical simulations and experimental studies are an important resource.

This works aims to show the relevance and mutual connection between the different design steps for what concerns the TES envelope, highlighting how simulation studies can help to define the required parameters (i.e., thermal conductivity threshold, insulation thickness) and how the experimental investigations on the materials can support the specific design of the envelope. The case of buried TTES vertical walls is investigated here, as many of the existing applications of large-scale PTES are non-insulated, thus making the definition of reliable designs and

insulation concepts an important research gap to be filled. In the design of TES envelope, material degradation due to combined effects of moisture and high temperatures is a non-negligible aspect. Structural elements in concrete, polymeric liners, piping systems and insulation need to be designed to enable high performance and long life. When considering the insulation, the high costs involved for both the material and the installation call for a careful selection and design based on a deep knowledge of the heat transfer phenomena involved. The insulating bore pile wall (IBPW) concept developed within the "gigaTES" project (van Helden et al., 2021) opens several questions concerning the optimal insulation material to be applied, the construction process and the final costs. Far from being able to answer all of these questions, this work aims to highlight the most important aspects to be taken into account in the material selection and envelope design, considering the thermophysical phenomena involved.

| (a) | (b) |
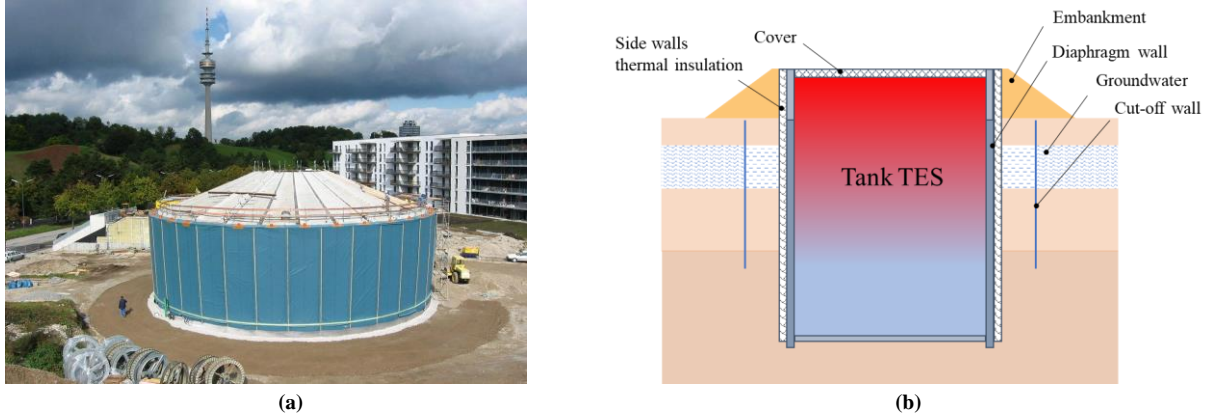
Fig 1: (a) Freestanding TTES in Munich Ackermannbogen. (b) Sketch of the main elements of a buried TTES with lateral insulation.

In this work an integrated approach for the assessment of the TES envelope properties is suggested. Alongside standard material tests, mock-ups replicating the specific application of vertical insulation in buried TTES are considered. Following the existing approach that uses thermal response tests (TRT) to determine the thermal properties of the ground (useful for the design of ground source heat pumps) (Spitler & Gehlin, 2015), a similar solution is implemented to study the performance of vertical underground insulation. Mock-ups for TES lateral insulations are built on a lab scale (to test the approach) and are followed by tests on field-scale underground mock-ups.

2. Materials and their properties

Among the different types of insulation materials, bulk granular insulation is considered to be a suitable solution that can be used as TES insulation due to its ease of installation without the need for scaffolding, as the grains can be poured and adjusted to any geometric irregularity. Some examples applied in existing TES are foam glass gravel (FGG), expanded glass granules and perlite. However, the heat transfer that occurs within the TES envelope goes beyond the thermal conduction, as radiation and convection can concur to increase significantly the heat flux, depending on the material's characteristics (granules vs. panels, porosity, permeability) and conditions (upwards/ horizontal heat flux, temperature difference) (Drück et al., 2022; Ochs & Bianchi Janetti, 2018). Due to the presence of open porosity (i.e. voids between the grains) and large temperature difference, the use of bulk granular insulation can be unfavorable from the point of view of insulation performance in the presence of upward and horizontal heat flow (as in the TES cover and wall, respectively), since the formation of natural convective transfer (which occurs as a consequence of the air density gradient) would represent a non-negligible part of the total heat flow. The negative effects of natural convection on the effective performance of thermal insulation have been observed in large-scale TES (Ochs, 2009), but affect also the insulation of spherical cryogenic storage tanks (Taghavi et al., 2024), making this a relevant research topic for various applications.

When investigating the heat transfer within the insulation layers, alongside the energy balance equation (eq. 1), the momentum equation needs to be included to solve the velocity field of the fluid (i.e., the air within the insulation layer) related to the convective heat transfer. For the application in porous insulation materials, the Brinkman equation can be introduced (eq. 2) as it describes the momentum transport in porous media.

$$\left(\rho C_p\right)_{bulk} \frac{\partial T}{\partial t} = \nabla \cdot (\lambda_{bulk} \nabla T) - \left(\rho C_p\right)_{bulk} u \cdot \nabla T \qquad \text{(eq. 1)}$$

$$\rho \frac{du}{dt} = \nabla \cdot \left[-pI + \frac{\eta}{\psi_{macro}}(\nabla u + (\nabla u)^T) + \frac{2}{3}\frac{\eta}{\psi_{macro}}(\nabla u)I\right] + \rho g \beta (T - T_c) + \frac{\eta}{K_{bulk}} u \qquad \text{(eq. 2)}$$

In the presented equations, T is the material temperature ([K]), ρ_{bulk} ([kg/m^3]) and $C_{p,bulk}$ ([J/(kg·K)]) the bulk density and thermal capacity, λ_{bulk} ([W/(m·K)]) the bulk thermal conductivity, u the fluid velocity within the bulk ([m/s]), ρ ([kg/m^3]) the fluid density, p ([Pa]) the pressure, η ([Pa·s]) the fluid viscosity, ψ_{bulk} the bulk macro porosity, β the expansion coefficient ([1/K]) and K_{bulk} ([m^2]) the bulk permeability.

Taking into account these phenomena in the TES modelling is computationally intensive, but the design process can be divided into different steps, each one focusing on a specific aspect of the design, as simplified in Fig. 2. System models based on TRNSYS or Modelica/Dymola can be used to define the TES capacity and operation temperatures, while detailed models based on MATLAB/Simulink or COMSOL Multiphysics can provide more detailed information concerning the required insulation performance and distribution (Ochs et al., 2022). For the detailed design of the single envelope components, software tools like COMSOL Multiphysics, ANSYS and Delphin can be used to model the heat, fluid and moisture transport within the materials. This numerical analysis can go on both directions (i.e., system-to-component and component-to-system) as the information gained on one level can be used on the others and viceversa. Experimental investigations are an additional important support to extend the knowledge of the material properties, investigate the application on small mock-ups of the TES elements, and provide important indications for the design process.
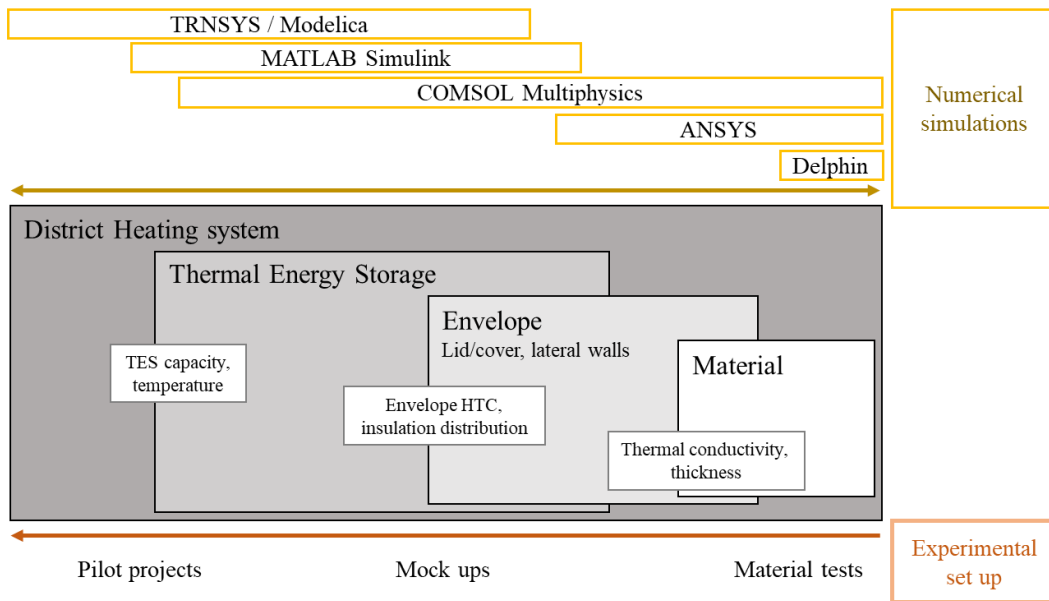

Fig. 2: Steps for the design of buried TES envelope.

3. Methodology

3.1. TES Numerical models

The integration of a buried TES within a DH systems is evaluated through the assessment of its performance under the expected operating conditions (i.e., charging/ discharging temperatures and profiles, seasonal/weekly operation). In this preliminary step, the surrounding ground (i.e., soil properties and stratification, presence of groundwater) can also be taken into account. Several numerical models are available for this type of evaluation (Ochs et al., 2022), depending on the degree of detail required and on the level of the analysis. This step is relevant to assess the general characteristics required from the TES envelope in terms of heat transfer coefficient (HTC). Many studies highlight the necessity to ensure a good performance of the insulation materials of the lateral walls, not only to improve the TES performance but also to reduce the impact on the surrounding ground and groundwater, depending on the material type (clay, sand, rock) but also on the groundwater depth and velocity (Dahash et al., 2021).

3.2. Assessment of materials' properties

Once the general requirements in terms of HTC are defined, the most suitable materials can be selected. The selection criteria for materials in this step include not only thermal conductivity, but also porosity, density, structure (panels, granules) and their attitude to absorb water. Material datasheets are an important source of information, but often the data are available for a limited range of temperatures, lower than the operation of the TES, that can reach 95 °C.

In order to assess the material behaviour at the specific operation conditions, and in particular the risk of natural convection development, three main approaches can be used: preliminary evaluations based on available data,

numerical modelling and material testing. Each one is to be considered complementary to the others, as they are able to provide different kind of information concerning the characteristics and performance of the material.

- *Preliminary assessment.* Alongside the material selection based on the properties available from the datasheets, a preliminary evaluation regarding the convection risk can be done using the Darcy-modified Rayleigh number presented in eq. 3 (Stephan et al., 2019), which defines the transition from conduction to convection (natural to turbulent) of the heat transfer in a porous material like thermal insulation.

$$Ra = \frac{g\,\beta_a}{\nu_a} \cdot \frac{L\,K\,\Delta T}{\alpha} \qquad \text{(eq. 3)}$$

The single contributions on the development of convective heat flux depend on fluid characteristics (ν_a is the fluid kinematic viscosity, [m²/s]), geometry and layout (L is the characteristic length [m], ΔT is the temperature difference between the two sides of the insulation [K]), and material characteristics (α thermal diffusivity [m²/s], K material permeability [m²]). Other factors are the gravitational acceleration (g, [m/s²]) and the coefficient of thermal expansion (β_a, [1/K]). The Rayleigh number allows to assess for different materials and applications (i.e., temperature difference and material thickness) the role of convection. Its limit is the fact that it considers a 1D heat transfer, while the heat transfer through TES lateral walls and cover is 2D or even 3D. Moreover, the material permeability is often an unknown parameter, that can be estimated through empirical correlations (see eq. 4, Ergun correlation (Ochs, 2009)) or experimentally defined, and the thermal conductivity used to the define the thermal diffusivity depends on the material average temperature, which is usually much higher than the temperature used to define the nominal thermal conductivity in commercial datasheets.

$$K_{Ergun} = \frac{d_m^2 \cdot \psi^3}{A \cdot (1-\psi)^2} \qquad \text{(eq. 4)}$$

- *Material testing.* Material investigations in this step consist in laboratory investigations to assess the thermal conductivity using one- and two-plates guarded hot plate (GHP) devices (Adam et al., 2015). The two-plates GHP device allows defining the thermal conductivity without the influence of convection, while the one-plate GHP device, depending on its orientation, allows to assess the relevance of convection with respect to conduction. These investigations allow to define the relation between thermal conductivity and temperature, that can be used for the Rayleigh evaluation.

- *Numerical modelling.* The material-level numerical modelling of the conducted tests allows defining the material permeability (also required for the Rayleigh evaluation) from the comparison with the experimental results (Ochs et al., 2015). Available tools are Delphin, specialized for the investigation of the moisture transport, and COMSOL Multiphysics, which is a FE-based software, able to solve multiphysics phenomena.
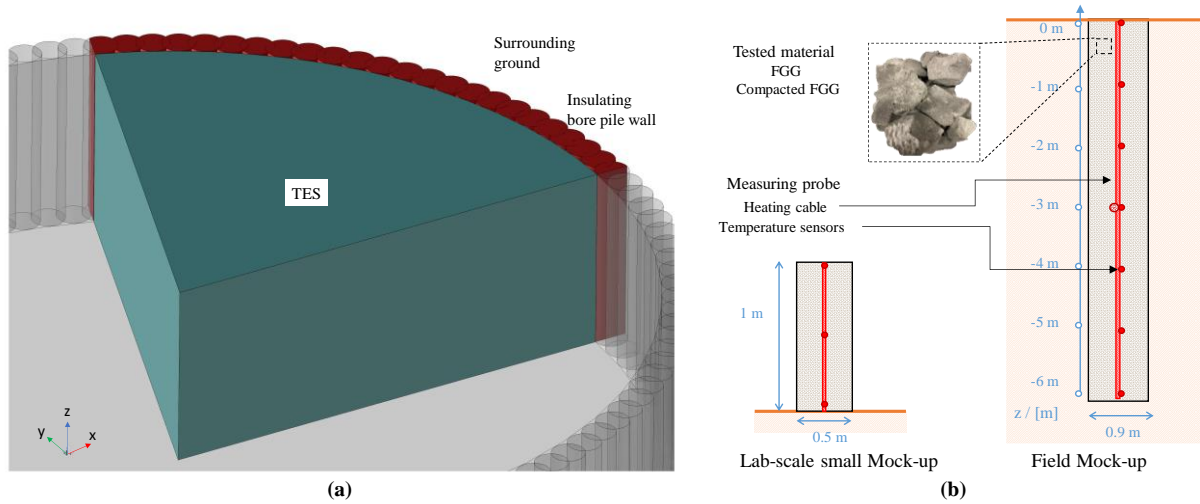
3.3. Mock ups

The knowledge of the material properties supports the definition of cost-effective insulation design solutions. In the IBPW concept, this additional step is used to assess the effective performance of the insulating material. The IBPW concept for the TTES vertical walls consists of a series of ground bored cylindrical piles filled with granular insulation (Tosatto, Ochs, Dahash, Muser, et al. (2022)), as presented in Fig. 3(a). The combination of porous granular insulation, high temperature differences (i.e., between the TES and the surrounding ground) and heat flux orientation (horizontal) will most likely trigger the development of a convective plume within the pile, thus resulting in an overall poorer insulation performance. The study of mock-ups allows for the investigation of the structural stability of the granular material (required to allow the over-drillability of the piles) and the optimization of the construction process (i.e., material mixing and compaction). In addition, the building physics performance of the selected material in the specific application can be tested and verified, thus providing further insights for the design optimization.

In the definition of the IBPW concept, the mock-up investigation is divided in two phases, one with lab-scale tests and one with field tests. Two mock-ups of an insulating pile are built: a small (lab-scale) insulating pile (small mock up, sMU) and a higher (drilled) insulating pile (field mock up, fMU), with the characteristics presented in Tab. 1 and the geometry presented in Fig. 3(b). Both mock-ups have the same experimental configuration, with a measuring probe located vertically along the symmetry axis of the cylindrical pile, containing an electric heating band and temperature sensors; the voids in the measuring probe are filled with sand. Within the "gigaTES" project, the tested insulation material is FGG, both compacted and uncompacted.

Tab. 1: Characteristics of the IBPW investigated mock ups.

	Small mock up	**Field mock up**
Height, [m]	1	6
Diameter, [m]	0.5	0.9
Type	freestanding	buried
Location	climate chamber (UIBK, AT)	construction site (Vienna, AT)
Tested materials	uncompacted and compacted FGG	

Fig. 3: Insulating bore pile solution for TES lateral walls. (a) Concept of the IBPW as lateral insulation. (b) Lab-scale and field mock-ups.

The testing procedure consists in a heating phase when the heating band is heated at a specific set point (80 to 90 °C to simulate TES operating temperatures), and a following cooling phase. The insulation performance of the investigated material is evaluated comparing the electric power required to maintain the given set point temperature and the profile of the temperature curve during the cooling phase. The experimental results are compared with numerical simulations, thus allowing to derive the apparent thermal conductivity and the permeability of the material at the specific conditions. Two numerical models are then implemented in COMSOL Multiphysics environment:

- a heat conduction model, which allows to assess the apparent thermal conductivity of the material. This simplified implementation of eq. 1 does not consider the convective term and is not able to capture all the involved phenomena, but provides a general evaluation concerning the insulation performance in terms of apparent thermal conductivity ($\lambda_{bulk,app}$, as from eq. 5), which considers both the heat transfer by conduction and convection.

$$\left(\rho C_p\right)_{bulk} \frac{\partial T}{\partial t} = \nabla \cdot \left(\lambda_{bulk,app} \nabla T\right) \qquad \text{(eq. 5)}$$

- a detailed model, able to consider also the convective heat transfer, combining the heat transfer (eq. 1) and the Brinkman equation (eq. 2), to estimate the bulk permeability.

The numerical models replicate the geometry and the boundary conditions of the two mock-ups and receive as input the (measured) electric power required by the heating band to maintain the desired set point temperature.

4. Results

4.1. TES numerical models

From existing studies based on numerical simulations of large-scale TES, HTC in the range of 0.2 W/(m²·K) to 0.3 W/(m²·K) are desirable to achieve sufficiently good TES storage efficiencies of 80-90 % depending on the TES volume and geometry. In presence of groundwater, lower overall HTCs are required (about 0.1 W/(m²·K)), together with additional geotechnical measures such as the installation of cut-off walls at an appropriate distance, in order to limit the groundwater temperature exceedance (Dahash et al., 2021).

4.2. Assessment of materials' properties

Given the output of the TES numerical simulations, in presence of groundwater an HTC around 0.1 W/(m^2·K) is desirable. To maintain the insulation layer thickness below 1 m (to minimize the required volume and the amount of material required), this results in a required thermal insulation effective conductivity around 0.1 W/(m·K). The reference to the 'apparent' thermal conductivity (eq. 5) rather than to the nominal one is necessary in the evaluation of the HTC, as it considers the total heat transfer, considering the additional influence of radiation and convection. Nevertheless, the nominal thermal conductivity provided by manufacturers is a good starting point to select the most suitable materials.

4.2.1. Material testing

The lab tests allow to investigate the effect of temperature on the material thermal conductivity under controlled boundary conditions. Previous tests run on FGG, both compacted and uncompacted, using a large one-plate GHP device (oriented downwards to prevent the development of convection) showed already a preliminary distinction between the two (Adam et al., 2015). The better performance of the compacted FGG can be traced back to the reduced impact of the radiative heat transfer, due to the reduced space between the grains. However, grain size, porosity distribution, relative humidity, probe thickness and temperature have a major influence on the heat transfer mechanisms and therefore on the measurement results. Therefore, the effects of convection, radiation and conduction (both in solid and in fluid domains) can compensate each other, leading to a higher uncertainty in the measurements (estimated to be around 5 %). For example, Mustafa et al. (2023) reported an opposite observation in the investigation of FGG, with increasing values of thermal conductivity with increasing compaction rates, but the measurement results were in a similar range as the ones reported by Adam et al. (2015).

The thermal conductivity of the investigated materials is defined as a linear function of the average temperature according to eq. 6, from the results presented by Adam et al. (2015). The nominal reference values for the two coefficients λ_a and λ_b are defined from material tests (see Fig. 4) at specific measuring points and extrapolated to higher temperatures. In addition to FGG, perlite is considered in the analysis as a reference material where convection plays a negligible role. In this case, thanks to the lower dimensions of the grains, a smaller one-plate GHP device (Taurus TCA 300, Taurus Instruments GmbH) was used, resulting in a smaller error.

$$\lambda_{bulk} = \lambda_a + \lambda_b \cdot T \quad \text{(eq. 6)}$$
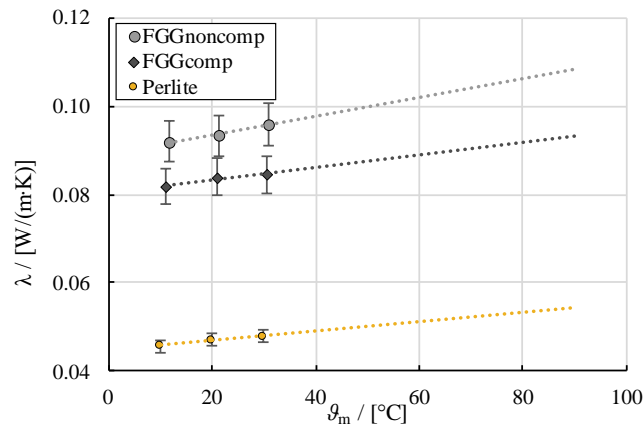

Fig. 4: Thermal conductivity for the investigated materials (FGG from (Adam et al., 2015)) as a function of the mean temperature.

4.2.2. Rayleigh number

The results provided by the material investigation (porosity, thermal conductivity as function of temperature), allow to derive a preliminary indication of the convection risk through the Rayleigh number. With the parameters presented in Tab. 2, the Rayleigh number is evaluated for the real scale application of the IBPW and for the two mock up solutions (sMU, and fMU). For this preliminary evaluation, the material permeability from the Ergun correlation (eq. 4) is used, while the fluid properties (i.e., air) are defined on the average temperature between the hot and the cold side.

Tab. 2: Input parameters for the evaluation of the Rayleigh number. The fluid properties are evaluated for the average temperature.

	Parameter	Perlite	FGG	Compacted FGG
Operation conditions	T (warm side) / [°C]		90	

	T (cold side) / [°C]	20		
	L / [m]	0.25 (sMU radius), 0.45 (fMU), 0.9 (IBPW)		
Insulation Material	λ / [W/(mK)]	$\lambda(T_m)$ (Fig. 4)		
	ψ / [-]	0.48	0.38	0.15
	d_m / [m]	0.003	0.35	0.35
	K_{Ergun} / [m²]	$2.4 \cdot 10^{-8}$	$1.16 \cdot 10^{-6}$	$7 \cdot 10^{-8}$
Fluid (air)	β / [1/K]	0.003		
	ρ / [kg/m³]	1.075		
	c_p / [J/(kgK)]	1007		
	ν / [m²/s]	$1.847 \cdot 10^{-5}$		

The resulting Rayleigh numbers, shown in Fig. 5, indicate that the influence of convection is expected to be more pronounced in the real scale application, since the main heat transfer occurs along the whole pile diameter, rather than along the radius (as in the two mock-ups where the heating cable is arranged axially). Considering the threshold of $Ra \approx 40$ proposed by Ochs et al. (2015) for the development of convection, the non-compacted FGG does not seem to be suitable for this specific application, while the compacted FGG solutions seem to be on the borderline, with the sMU below the convection risk threshold, and the larger structures (fMU and real scale IBPW) susceptible to the risk of convection development. An important element of uncertainty is in the assessment of the permeability of the porous bulk, which depends on the degree of compaction and its distribution, which may not be homogeneous within the probe.
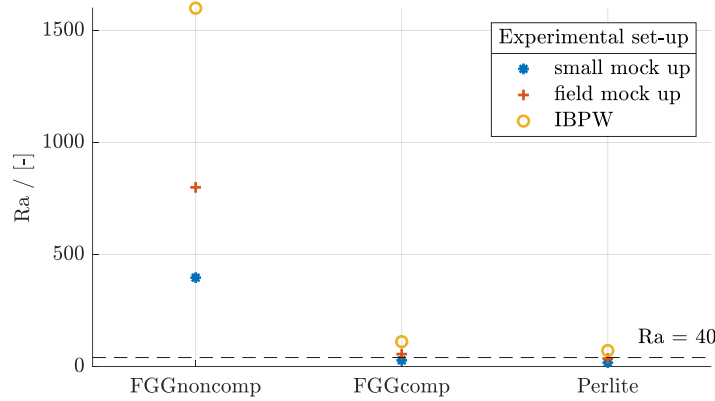

Fig. 5: Rayleigh number for the IBPW: small mock up, field tests and real scale application and threshold for the risk of convection.

4.3. Mock up

The investigation of the insulation material performance in a configuration similar to the final application helps to define the most suitable installation procedures and to evaluate potential challenges in this phase. In order to cross-check the results of the Rayleigh evaluation and to provide a reference test procedure for the IBPW, two mock-up solutions are investigated: a lab-scale sMU and a larger scale fMU.

The indicators used to assess the performance of the different configurations are:

- the effective electric power required to maintain the set point temperature (eq. 7). This is directly measured from the test and provides an immediate indicator (P_{el} is used as input in the implemented numerical model).

$$P_{eq} = \frac{P_{el}}{H_{pile} \cdot (T_{max} - T_{min})} \qquad \text{(eq. 7)}$$

- the apparent thermal conductivity of the material (eq. 5), resulting from the comparison between the measured temperatures and the numerical simulation results.

- the Rayleigh number, derived from the assessment of the bulk permeability with the detailed model.

A reference test using perlite in the sMU, is run to calibrate the numerical model and to provide a reference value for the FGG. Fig. 6 shows the geometry of the model implemented in COMSOL Multiphysics for the sMU; thanks to

the axial symmetry of the mock-up, the numerical model was built using a 2D axisymmetric geometry. Tab. 3 presents the properties of the probe materials defined with the reference test and used in the following simulations.
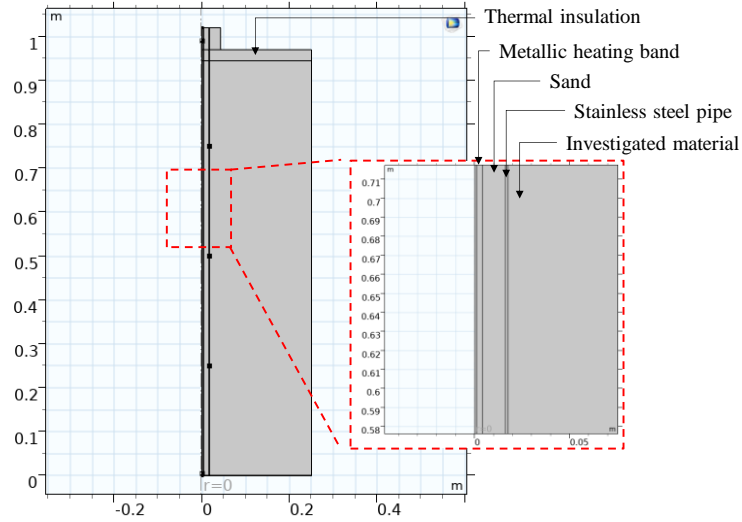

Fig. 6: Axisymmetric view of the sMU implemented in COMSOL Multiphysics.

Tab. 3: Probe parameters defined from model calibration.

Material	Thermal conductivity, λ [W/(m·K)]	Thermal capacity, $(\rho \cdot c_p)$ [J/(kg·m^3)]
Metallic heating band	200	2.40e+06
Sand	1	1.26e+06
Stainless steel pipe	30	4.16e+06

The comparison between measured and simulated temperature curves of the mock ups allows to define the apparent thermal conductivity, by changing the coefficient $\lambda_{a,app}$ in the heat conduction model (see eq. 8), while in the detailed model with Brinkman equations the permeability K is evaluated, using the nominal λ_{bulk} from eq. 6.

$$\lambda_{app} = \lambda_{a,app} + \lambda_b \cdot T \qquad \text{(eq. 8)}$$

Fig. 7(a) presents the measured effective powers for the conducted tests and Fig. 7(b) the measured temperature profiles for the three investigated materials. From fig. 7(a) it is possible to see the better insulation performance of perlite, which has the lowest nominal thermal conductivity and requires a lower power to maintain the set point temperature of 90 °C during the heating phase compared to the uncompacted FGG, which shows the worst performance. From the temperature profiles in Fig. 7(b), the influence of convection in the uncompacted FGG is visible, with the upper temperature sensor measuring the highest temperatures, while perlite and compacted FGG measure higher temperatures in the central probe.
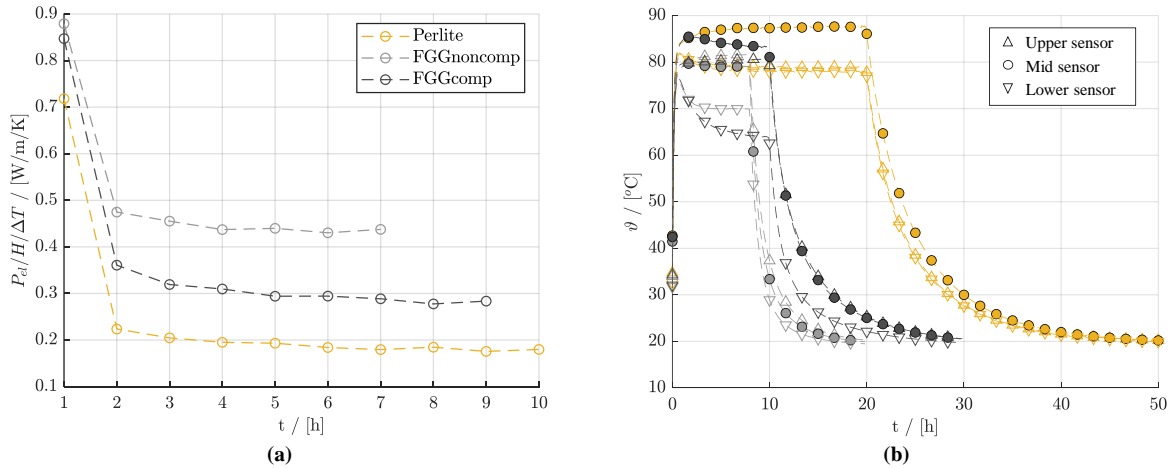

Fig. 7: (a) Effective electric power required to maintain the set point temperature. (b) Measured temperature profiles.

For the assessment of the material apparent thermal conductivity, the measured temperature profiles are compared to the simulated ones. The results of the heat conduction model are presented in Fig. 8 for the sMU, for the reference measurement with perlite and the two FGG cases (non-compacted and compacted), for the mid sensor only, as border and 3D effects on the upper and lower sensor make it difficult to conclude on the respective simulation results.

It is possible to see that the pure heat conduction model is able to replicate quite well the behavior of the material in presence of low or negligible convective heat transfer. Therefore, the simulated temperature curves of perlite and compacted FGG are quite close to the measured values, with the best match with $\lambda_{a,app}$=0.04 W/(m·K). In case of the perlite (used as reference measurement to calibrate the model), the uncertainty in the $\lambda_{a,app}$ term is around 0.005 W/(m·K), which is considered acceptable taking into account the complexity of the geometry and the uncertainty in the properties of the insulating probe used in the numerical model.

In case of the non-compacted FGG, the curve which enables the best fit with the measured values is $\lambda_{a,app}$=0.2 W/(m·K), as already observed by Tosatto, Ochs, Dahash, Muser, et al. (2022). This means, that against a nominal thermal conductivity of around 0.09 W/(m·K) (see Fig. 4), the apparent conductivity, taking into account the effect of convection, is at least double. In the compacted FGG, material compaction, through the reduction of the bulk porosity, does not only reduce the convective heat transfer, but also the radiative, resulting in $\lambda_{a,app}$ of around 0.1 W/(m·K).
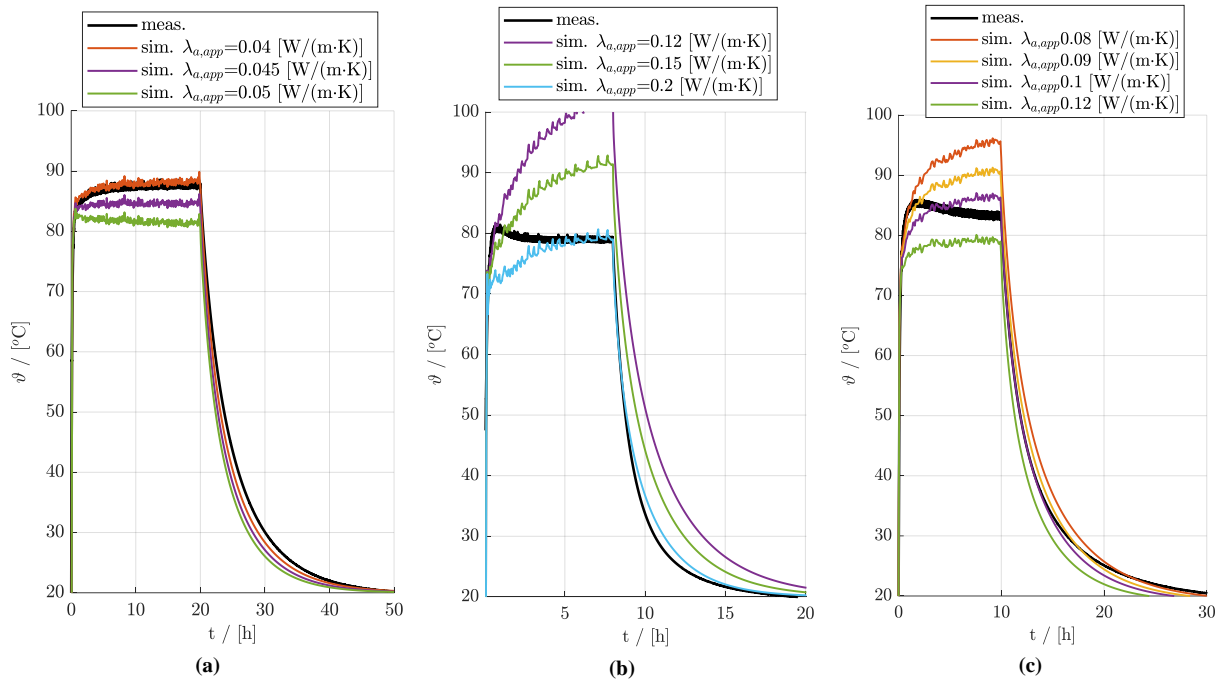
Fig. 8: Apparent thermal conductivity evaluation with heat conduction model. (a) Perlite (b) FGG non-compacted. (c) compacted FGG.

However, the heat conduction model alone is not able to capture the dynamics of the heat transfer. In porous media, thermal conductivity increases with increasing temperature as the air conductivity increases, but radiative heat transfer also plays a role as temperature differences increase, and air motion due to buoyancy results in an inhomogeneous radial and vertical temperature distribution. The use of a detailed model capable of simulating also the fluid motion is useful to investigate the effects of convection and to take into account the properties of the air. Fig. 9 presents the temperature profiles of the mid sensor, obtained with the detailed numerical model. It is possible to observe that this model allows to better capture the dynamics of the measurement, especially in the heating phase. The permeability that allows the best fit is $7 \cdot 10^{-7}$ m² in the case of the non-compacted FGG and $1 \cdot 10^{-7}$ m² in the case of the compacted FGG, which are comparable to the values derived empirically using the Ergun correlation (presented in Tab. 2). In the case of the sMUs, the results obtained in the preliminary evaluation using the Rayleigh number (Fig. 5) are then confirmed by the lab tests.
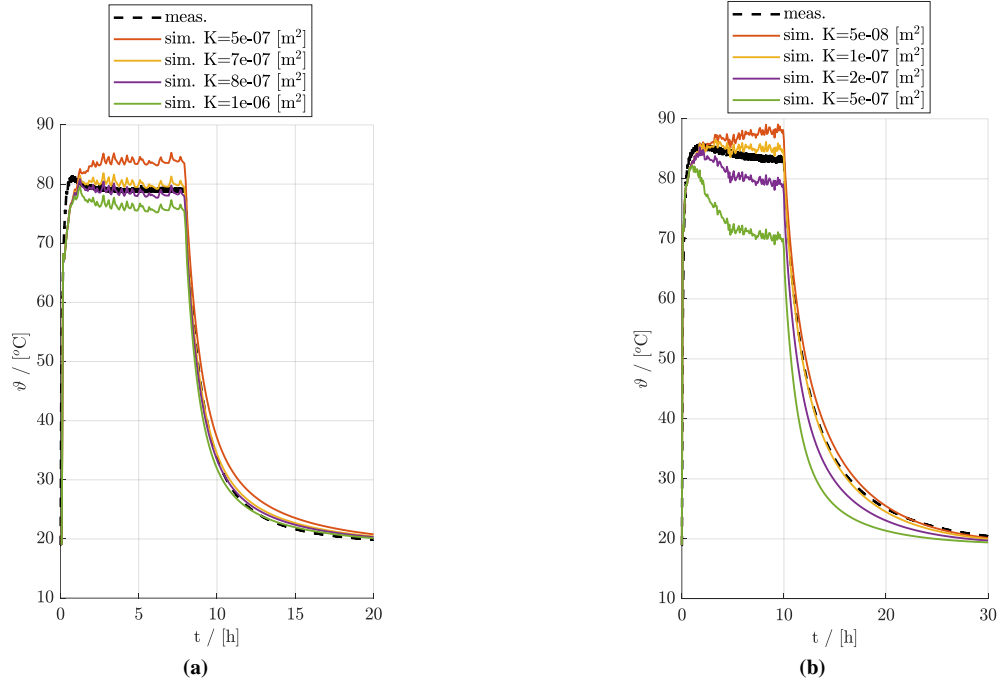
Fig. 9: Permeability evaluation with detailed numerical model. (a) FGG non-compacted. (b) compacted FGG.

The extension of the study on the field tests allows to investigate how the larger dimensions of the probe (both in terms of height and diameter), affect the development of convection, as suggested from the Rayleigh number evaluation. This is visible from the effective electric power required to maintain the set point temperature, presented in Fig. 10. The larger mass of the piles in the field tests require a longer heating phase to reach steady state conditions to compare the required powers. The compacted FGG configuration shows a better performance than the uncompacted one, but in the fMU it is worse than that observed in the sMU. This difference can be attributed to two main reasons: (1) in the sMU, homogeneous compaction is ensured as the FGG is compacted layer by layer under visual control, whereas in the fMU, different layers may have different degrees of compaction and therefore different permeability, (2) the larger radius of the fMU favors the development of the convective plume.

The field tests thus made it possible to observe how the construction procedure has an influence on the insulating performance of the material. Inhomogeneous compaction results in higher porosity along the vertical, thus favoring convection in already critical conditions (due to the larger dimensions).
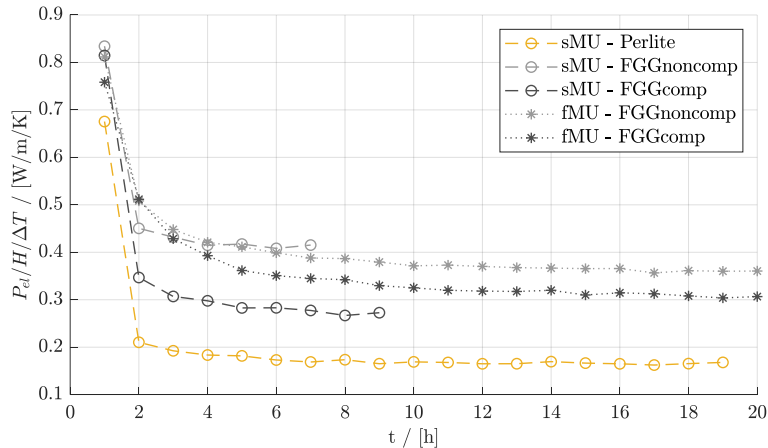

Fig. 10: Effective electric power required to maintain the set point temperature in the sMU and fMU.

5. Conclusions

In this work, the role of numerical studies and experimental studies is defined in supporting the design of the envelope and insulation of buried TES. Both can be divided in different steps, going from the smallest element (i.e., the material itself) to the component (i.e., the TES vertical wall or cover) to the system. Each of these steps is able to provide indications about the envelope requirements and the specific characteristics that the materials need to have, thus helping the designer selecting the ideal insulation material and ensuring that it performs as intended.

The specific case of IBPW is here presented as example. TES-level studies are able to define a range for the required HTC to ensure both a good TES performance (in terms of thermal losses) and prevent the groundwater overheating. Bulk insulation materials appear to be the most suitable for this kind of application, and the minimum required insulation thickness can be defined from their nominal thermal conductivities. The effective performance of these materials can however deviate from the one provided by the manufacturers' datasheets, as high temperatures and horizontal/upwards heat fluxes can trigger the development of convection, thus enhancing the local heat transfer. Targeted material testing and insulation mock ups are able to assess the performance of the materials under the TES operation conditions and to give indication about the optimal construction process. FGG is one of the most suitable materials for this application, thanks to its high structural stability and its good insulation performance. The large porosity within the FGG bulk makes it however prone to the development of convection in presence of high temperature difference and unfavorable heat transfer direction: material compaction can block the convection, but it may not be sufficient in the real-scale application, as observed both by theory analysis (Rayleigh number) and targeted material tests. The field tests confirmed the preliminary investigations with the Rayleigh number in terms of convection risk development and provided important insights on the structural stability of the insulation material to ensure the over-drillability. Further studies within the "ScaleUp" project are ongoing and investigate the possibility to mix different granular insulation materials with different granulometries to prevent the convection development.

6. Acknowledgments

7. References

Adam, D., Andreatta, A., Feist, W., & Feix, J. (2015). Grundlagenforschung Glasschaumgranulatschüttungen als lastabtragender und wärmedämmender Baustoff - Berichte aus Energie- und Umweltforschung. In *Bundesministerium für Verkehr, Innovation und Technologie*.

Dahash, A., Ochs, F., Giuliani, G., & Tosatto, A. (2021). Understanding the interaction between groundwater and large-scale underground hot-water tanks and pits. *Sustainable Cities and Society*, *71*, 102928. https://doi.org/10.1016/j.scs.2021.102928

Drück, H., Bonk, N., Juschka, W., Ullmann, J., Lang, S., Gensbaur, M., Bestenlehner, D., Hübner, J., Reu, E., & Abel, S. (2022). *Erweiterung und Optimierung der solaren Nahwärmeversorgung Hirtenwiesen II in Crailsheim sowie Begleitforschung zu solarer Nahwärme und saisonaler Wärmespeicherung (CROW)*. 1–130.

Golmohamadi, H., Larsen, K. G., Jensen, P. G., & Hasrat, I. R. (2022). Integration of flexibility potentials of district heating systems into electricity markets: A review. *Renewable and Sustainable Energy Reviews*, *159*, 112200. https://doi.org/10.1016/J.RSER.2022.112200

International Energy Agency (IEA). (2024). *IEA ES TCP Task 39 - Large Thermal Energy Storages for District Heating. Deliverable A5 - List of LTES projects*. https://iea-es.org/task-39/deliverables/

Mustafa, W. S., Szendefy, J., & Nagy, B. (2023). Thermal Performance of Foam Glass Aggregate at Different Compaction Ratios. *Buildings*, *13*(7), 1844. https://doi.org/10.3390/buildings13071844

Ochs, F. (2009). *Modelling Large-Scale Thermal Energy Stores* [Univ. Diss.]. University of Stuttgart.

Ochs, F., & Bianchi Janetti, M. (2018). *Wärmeleitfähigkeit von Dämmstoffen in Abhängigkeit von Temperatur und Feuchtegehalt. In: Stephan, P., Mewes, D., Kabelac, S., Kind, M., Schaber, K., Wetzel, T. (eds) VDI-Wärmeatlas*. Springer Vieweg, Berlin, Heidelberg. https://doi.org/10.1007/978-3-662-52991-1_107-1

Ochs, F., Bianchi Janetti, M., & Klesnil, O. (2015). *Wärmeleitfähigkeit von Schüttungen aus Glasschaumgranulat: Messtechnische Analyse sowie Analytische und Numerische Modellierung*. http://www.aee-now.at/cms/fileadmin/downloads/projekte/store4grid/store4Grid Wärmeleitfähigkeit.pdf

Ochs, F., Dahash, A., Tosatto, A., Reisenbichler, M., O'Donovan, K., Gauthier, G., Kok Skov, C., & Schmidt, T. (2022). Comprehensive Comparison of Different Models for Large-Scale Thermal Energy Storage. *Proceedings of the International Renewable Energy Storage Conference 2021 (IRES 2021)*, 36–51. https://doi.org/10.2991/ahe.k.220301.005

Schmidt, T., Pauschinger, T., Sørensen, P. A., Snijders, A., Djebbar, R., Boulter, R., & Thornton, J. (2018). Design Aspects for Large-scale Pit and Aquifer Thermal Energy Storage for District Heating and Cooling. *Energy Procedia*, *149*, 585–594. https://doi.org/10.1016/j.egypro.2018.08.223

Spitler, J. D., & Gehlin, S. E. A. (2015). Thermal response testing for ground source heat pump systems—An historical review. *Renewable and Sustainable Energy Reviews*, *50*, 1125–1137. https://doi.org/10.1016/J.RSER.2015.05.061

Stephan, P., Kabelac, S., Kind, M., Mewes, D., Schaber, K., & Wetzel, T. (Eds.). (2019). *VDI-Wärmeatlas. Fachlicher Träger VDI-Gesellschaft Verfahrenstechnik und Chemieingenieurwesen* (12th ed.). Springer Vieweg Berlin, Heidelberg. https://doi.org/https://doi.org/10.1007/978-3-662-52989-8

Taghavi, M., Sharma, S., & Balakotaiah, V. (2024). Natural convection effects in insulation layers of spherical cryogenic storage tanks. *International Journal of Heat and Mass Transfer*, *220*. https://doi.org/10.1016/j.ijheatmasstransfer.2023.124918

Tosatto, A., Ochs, F., Dahash, A., & Muser, C. (2022). The Challenge of Planning and Constructing Large-Scale Hot Water TES for District Heating System: A Techno-Economic Analysis. *Proceedings of the International Renewable Energy Storage Conference 2021 (IRES 2021)*, 52–66. https://doi.org/https://doi.org/10.2991/ahe.k.220301.006

Tosatto, A., Ochs, F., Dahash, A., Muser, C., Kutscha-Lissberg, F., & Kremnitzer, P. (2022). Insulating piles for the cost-effective construction of very large-scale high temperature thermal energy storage. *Proceedings of the International Renewable Energy Storage Conference 2021 (IRES 2021)*, 67–77. https://doi.org/https://doi.org/10.2991/ahe.k.220301.007

van Helden, W., Leusbrock, I., O'Donovan, K., Reisenbichler, M., Riegler, T., Knabl, S., Wallner, G. M., Peham, L., Pugstaller, R., Muser, C., Drucker, P., Moser, M., Ochs, F., Tosatto, A., Dahash, A., & Bianchi Janetti, M. (2021). *Giga-scale thermal energy storage for renewable districts - Publishable final report*. https://www.gigates.at/index.php/en/publications/reports